









Budgeting the emittance of photoemitted electron beams in a space-charge affected emission regime for free-electron laser applications

Cite as: AIP Advances 10, 035017 (2020); <https://doi.org/10.1063/1.5129532>

Submitted: 29 September 2019 . Accepted: 28 February 2020 . Published Online: 13 March 2020

Y. Chen , M. Krasilnikov , M. Gross , P. Huang, I. Isaev, C. Koschitzki, X.-K. Li, O. Lishilin , G. Loisch , R. Niemczyk , A. Oppelt , H.-J. Qian, G. Shu, F. Stephan , and G. Vashchenko



View Online



Export Citation



CrossMark

ARTICLES YOU MAY BE INTERESTED IN

[Laser polishing of tool steel using a continuous-wave laser assisted by a steady magnetic field](#)

AIP Advances 10, 025319 (2020); <https://doi.org/10.1063/1.5116686>

AVS Quantum Science

Co-Published by



RECEIVE THE LATEST UPDATES



Budgeting the emittance of photoemitted electron beams in a space-charge affected emission regime for free-electron laser applications

Cite as: AIP Advances 10, 035017 (2020); doi: 10.1063/1.5129532

Submitted: 29 September 2019 • Accepted: 28 February 2020 •

Published Online: 13 March 2020



Y. Chen,^{a)} M. Krasilnikov,^{b)} M. Gross, P. Huang, I. Isaev, C. Koschitzki, X.-K. Li, O. Lishilin, G. Loisch, R. Niemczyk, A. Oppelt, H.-J. Qian, G. Shu, F. Stephan,^{c)} and G. Vashchenko

AFFILIATIONS

Deutsches Elektronen-Synchrotron DESY, 15738 Zeuthen, Germany

^{a)} Author to whom correspondence should be addressed: ye.lining.chen@desy.de

^{b)} Electronic mail: mikhail.kraskilnikov@desy.de

^{c)} Electronic mail: frank.stephan@desy.de

ABSTRACT

Free-electron laser based x-ray facilities require high-brightness photoinjectors to provide low emittance electron beams at a fixed bunch charge. The emittance optimization in the injector determines the lowest achievable emittance. Based on experimental emittance optimization at the photoinjector test facility at DESY in Zeuthen, a space-charge affected emission regime is identified, in which the optimum transverse beam emittance is achieved and thus, the injector is routinely operated in this regime. An advanced modeling approach is proposed to consider a dynamic emission process in the simulation of injector beam dynamics, meanwhile allowing detailed studies of the impact of strong space-charge fields during emission on the slice formation of the emitted electron bunch at the cathode. As an application, the proposed approach is used to analyze the budget of the optimized transverse beam emittance. An interplay, taking place in the identified emission regime, between intrinsic cathode emittance and space-charge induced emittance is demonstrated. The resolved behavior by simulation is consistent with the corresponding measurement under practical operation conditions of interest. The obtained results are reported.

© 2020 Author(s). All article content, except where otherwise noted, is licensed under a Creative Commons Attribution (CC BY) license (<http://creativecommons.org/licenses/by/4.0/>). <https://doi.org/10.1063/1.5129532>

I. INTRODUCTION

Free-Electron Laser (FEL) based x-ray facilities¹ are prevalently required by science-driven interdisciplinary proposals.² Such facilities demand the photoinjectors to provide high-brightness electron beams. For a fixed bunch charge, this entails minimization of the beam emittance in all planes. The lowest achievable emittance for linac-based accelerators is, however, already set at the injector exit, giving the emittance optimization in the injector a crucial role.^{3,4} The emittance budget mainly consists of the contributions from the space-charge and Radio Frequency (RF) forces, and the photocathode, as well as the coupling terms between each other. Among these emittance contributions, the

intrinsic emittance of the cathode sets the lower limit of the overall emittance.^{5,6}

II. OBSERVATION OF OPTIMIZED EMITTANCE IN A SPACE-CHARGE AFFECTED EMISSION REGIME

A. Emittance optimization scheme

An experimental optimization scheme of the normalized transverse beam emittance at the photoinjector test facility at DESY in Zeuthen (PITZ)⁷ is described as follows: First, the emittance is measured using a slit-scan technique⁸ as a function of the gun solenoid current at a given transverse spot size of the cathode drive laser pulse.

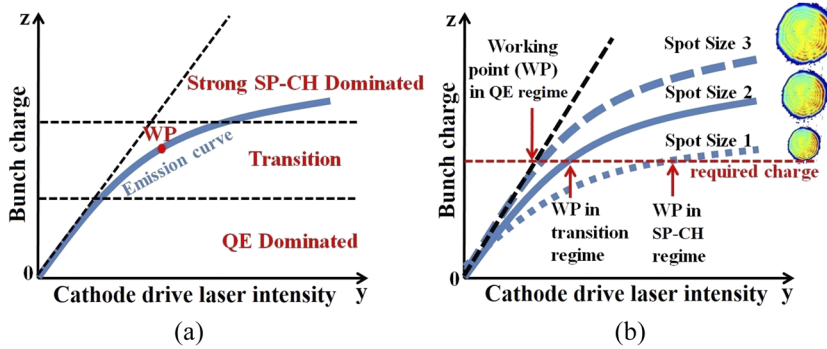


FIG. 1. Sketch of a characteristic emission curve (a) and concepts of emission regimes when applying different cathode laser spot sizes for emittance optimization (b). The inset transverse laser distributions in (b) are only used to illustrate the size change in the cathode laser spot. Note that the two horizontal dashed lines in (a) illustratively separate different emission regimes while the other dashed line shows a linear trend of the emission curve when the cathode laser intensity is relatively low.

Second, the spot size of the laser pulse is optimized for the smallest achievable emittance. The temporal laser pulse shape and length are kept invariant for simplicity. In addition, a so-called emission curve, defined as the emitted bunch charge vs the cathode drive laser intensity, is routinely measured at PITZ.

B. Space-charge affected emission

Figure 1(a) shows a sketch of an emission curve. As the cathode drive laser intensity increases, the emission curve is bent by space-charge effects. This generally separates the emission curve into different regimes,⁹ Quantum Efficiency (QE) dominated regime, transition regime,¹⁰ and strong SPace-CHarge (SP-CH) dominated regime, respectively. The red dot on the emission curve corresponds to a typical Working Point (WP) of the accelerator. As the working point lies on the non-linear part of the emission curve, the beam dynamics in the transition regime is already influenced by the space-charge effects. As described before, for emittance optimization, the transverse spot size of the cathode laser pulse is varied, resulting in a tendency change in the emission curve due to the variation of the local space-charge density at the cathode. This

is illustrated in Fig. 1(b), where three emission curves are exemplarily sketched for three different laser spot sizes. As shown in Fig. 1(b), for producing a required bunch charge (red dashed line), the Working Points (WPs) for various laser spot sizes settle in different regimes of photoemission, namely, the QE dominated (left), the transition (middle), and the SP-CH dominated (right) regimes, respectively.

C. Experimental observation

When the accelerator is operated at the transition regime of photoemission, the best beam emittance is observed in the experiment. This is exemplarily shown in Fig. 2. The measured emittance is optimized at the chosen WP (blue dot) in the transition emission regime for 1 nC bunch charge when the maximum cathode field gradient is about 60 MV/m. Such findings are routinely observed in the experiments for various machine operation conditions.^{7,11} The transition regime of emission is critical for improving the performance of photoinjectors. However, the associated dynamics in this regime cannot be reproduced well by simulations.¹² Discrepancies of beam parameters exist between measurement and simulation.^{7,11,13}

III. CHARGED PARTICLE DYNAMICS WITH PHOTOEMISSION MODELING

To understand the particle dynamics in the transition regime of emission, an advanced approach is proposed by modeling the emission process based on cathode physics. This is done, more specifically, by incorporating an emission model with a particle tracking code. Based on Spicer's three-step photoemission theory,¹⁴ the incorporated emission model^{15–17} originally developed by Jensen is further enhanced to take into account collective effects in the cathode vicinity.¹⁸ A simplified Quantum Efficiency (QE) formalism of the cathode reads

$$QE[\Phi_{\text{eff}}(r_{\perp}, t)] = \frac{\alpha}{\{1 + E_a/[\hbar\omega - \Phi_{\text{eff}}(r_{\perp}, t)]\}^2}, \quad (1)$$

with

$$\Phi_{\text{eff}} = \Phi_0 \pm \Phi_s \quad (2)$$

and

$$\Phi_s = e\sqrt{e[E_{\text{rf}}(r_{\perp}, t, z=0) + E_{\text{sc}}(r_{\perp}, t, z=0)]/4\pi\epsilon_0}. \quad (3)$$

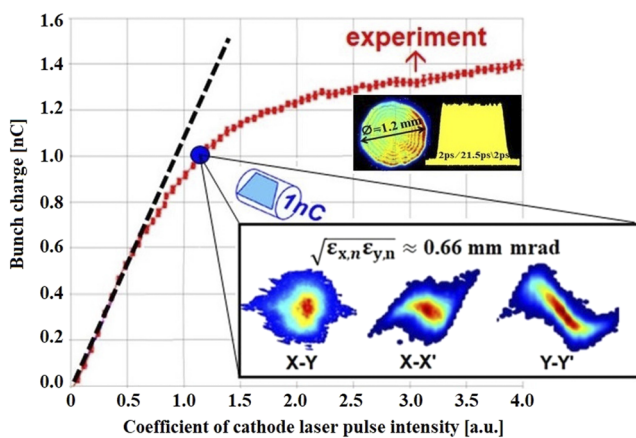


FIG. 2. A measured emission curve for a Cs₂Te photocathode under standard operation conditions⁷ of the PITZ accelerator. The insets show the used transverse (upper left) and temporal cathode laser distributions (upper right), the measured transverse beam profile (lower left), and phase spaces (lower middle and right).

The form factor in Eq. (1) $\alpha = \eta/(1 + p)$ with p physically interpreting the ratio of the drive laser penetration depth to the average distance an electron travels between collision events and η defined as a coefficient in proportion to the reflectivity of the cathode surface. The symbol E_a denotes the electron affinity, and the term Φ_{eff} represents the effective cathode work function for describing the probability of electron escape from the cathode surface by overcoming the surface barrier potentials. The latter is further decomposed to the intrinsic cathode work function, Φ_0 , and the modification of the intrinsic contribution by Φ_s due to the presence of strong fields on the cathode surface through a Schottky-like effect, as described in Eqs. (2) and (3). For semiconductor cathodes (e.g., Cs₂Te), the intrinsic work function is typically expressed as the sum of electron affinity, E_a and bandgap, E_g . The symbols e and ϵ_0 in Eq. (3) denote electron charge and vacuum permittivity, respectively. The terms E_{rf} and E_{sc} stand for the spatial (r_{\perp}) and temporal (t) dependent energy parameters of the RF and beam self-fields at the cathode position, respectively. The symbol “ \pm ” in Φ_{eff} marks the moment when the full field (i.e., $E_{\text{rf}} + E_{\text{sc}}$) changes its sign at the cathode surface position ($z = 0$). Based on Eqs. (1)–(3), the transient charge production is expressed as

$$dQ(r_{\perp}, t) = \frac{e\alpha dE_{\text{las}}(r_{\perp}, t) dr_{\perp} dt}{\hbar\omega \{1 + E_a/[\hbar\omega - \Phi_{\text{eff}}(r_{\perp}, t)]\}^2}, \quad (4)$$

where dE_{las} represents the energy of the cathode drive laser pulse and $\hbar\omega$ stands for the photon energy. The extracted total charge is then computed as the integration of Eq. (4) over the laser-illuminated area on the cathode surface during emission.

The emission model aforementioned is incorporated with a 3D full electromagnetic Lienard–Wiechert approach^{19–21} for particle dynamics simulations. A measurement-data-based training scheme¹¹ is applied to determine the form factor in the emission model. An initial particle distribution is generated according to the convolution of the realistic (measured) transverse cathode drive laser temporal intensity distribution and the measured cathode QE

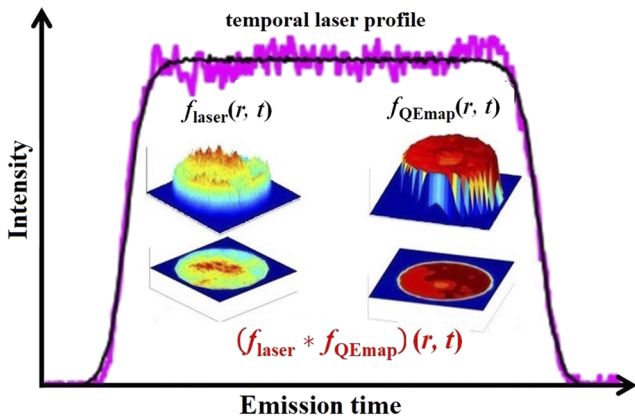


FIG. 3. Particle distribution generation by the convolution of the measured cathode drive laser temporal intensity distribution and the measured cathode QE map during emission. Pink curve: typically measured temporal laser intensity profile. Black curve: shape-preserving fit for the measurement. The inset distributions show exemplarily the measured transverse distribution of the cathode laser pulse and the measured QE map of the cathode.

map within the emission time, as shown in Fig. 3. By introducing the field-dependent cathode work function [Eqs. (1)–(4)] into the particle tracking approach, a time and space dependent dynamic emission process is made possible, allowing studies of the slice formation of the extracted electron bunch at the cathode, and allowing more detailed simulations of the beam parameters in the transition regime of emission. The follow-up intrinsic emittance calculation follows the work by Floettmann.²²

IV. SPACE-CHARGE AFFECTED INTRINSIC SURFACE EMITTANCE AT CATHODE

Figure 4 shows four defined working points (WPs) along a measured emission curve for specifically setting up the simulation of beam intrinsic emittance in Fig. 5. Varying the WP from A to D corresponds to the increase in the energy of the cathode drive laser pulse which implies the increase in the local charge density at the cathode plane. Figure 5 shows the intrinsic emittance on the cathode surface at different WPs, A–D. As shown in the figure, an intra-bunch modulation is observed at the WPs B–D. This is due to the fact that strong space-charge fields on the cathode surface increase the cathode work function and decrease the excess energy of the photoemitted electrons. The effect is stronger and starts to develop earlier for a higher local charge density at the cathode. It is exemplarily demonstrated in this case that the effect results in a 30% peak-to-peak reduction of the intrinsic bunch emittance and correspondingly, a 10% drop in the average emittance for different WPs in Fig. 4. In addition, as shown in Fig. 2, the optimum working point of the accelerator is typically located in the transition regime of photoemission, and in such a regime (e.g., at WPs C and D in Fig. 4) strong modulations of the intrinsic emittance are observed (Fig. 5). This means, the modulation effect of the intrinsic emittance needs to be considered in beam dynamics simulations in the transition regime of emission for properly budgeting the optimized emittance.

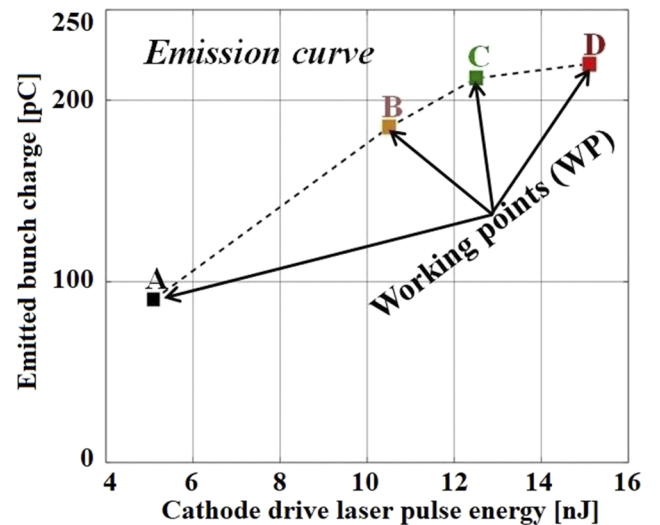


FIG. 4. Working points defined along a measured emission curve for the simulation of intrinsic surface emittance in Fig. 5.

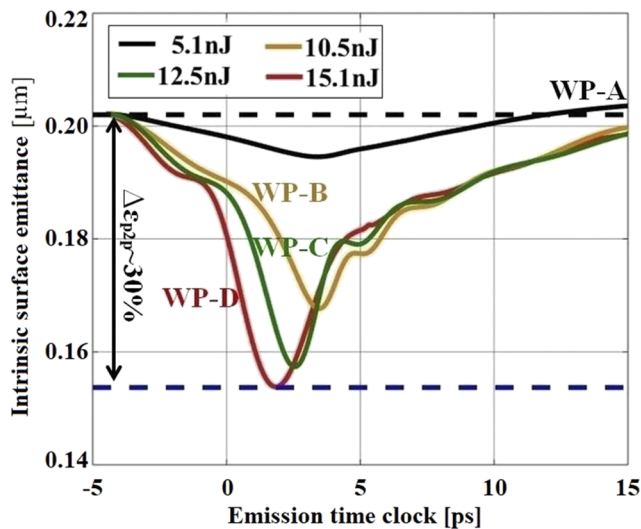


FIG. 5. Intrinsic surface emittance at the cathode vs emission time clock.

V. BUDGETED OVERALL TRANSVERSE EMITTANCE

Using the proposed approach, the emittance budget in the transition regime of photoemission is numerically and experimentally investigated. As for basic setups, the PITZ gun is operated to yield a maximum electric field of 40 MV/m at the photocathode. The launch RF phase is tuned to the phase corresponding to the maximum mean momentum gain. The Cut-Disk-Structure (CDS) booster is operated on-crest, resulting in a final beam mean momentum of about 18 MeV/c. A cathode laser pulse with a temporal Gaussian profile of about 6 ps full width at half maximum is used for this study. More detailed description can be found in recent studies at PITZ.²³

In Fig. 6, the emission curves are measured for three different transverse laser spot sizes of 0.5 (black), 0.7 (blue), and 0.9 mm (pink) in diameter. As shown in the figure, as the transverse spot size decreases, the WP for extracting the required bunch charge of 100 pC (horizontal dashed line) evolves from the QE dominated regime to the transition regime until the strong SP-CH dominated emission regime. At these WPs, the transverse beam emittance is measured and simulated correspondingly, as shown in Fig. 7. The experimentally optimized transverse emittance is achieved at the optimum spot size of 0.7 mm (black curve). The observation that the optimum working point is located in the transition regime of photoemission is consistent with the finding in Fig. 2, where the measurement was done for a higher bunch charge (1 nC). Compared to the WPs in the QE dominated (at 0.9 mm) and the strong SP-CH dominated (at 0.5 mm) emission regime, this demonstrates, once again, that working point at the transition regime delivers the best optimized beam emittance. The simulation result with emission modeling of the field-dependent cathode work function (blue curve) shows a better agreement with the measurement data when compared to the case without the modeling approach (red curve). The simulated emittance is closer to the measured value, and more importantly, the predicted optimum transverse cathode laser spot size is the same as the measured one.

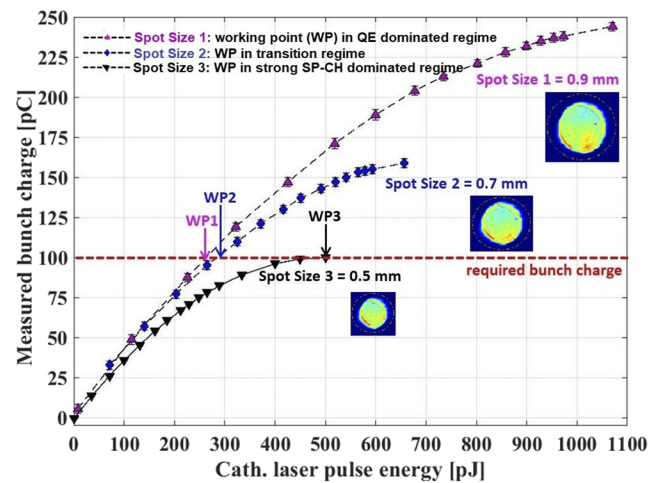


FIG. 6. Working points defined on three measured emission curves for emittance optimization at 100 pC. The plots show the measured transverse distributions of the cathode drive laser pulses with different spot sizes.

Furthermore, the overall emittance budget is analyzed. The red and green bars (Fig. 7, right axis) indicate the space-charge induced emittance and the intrinsic cathode emittance, respectively, for different cathode laser spot sizes (i.e., different working points in terms of emission regimes). It is clearly seen, that when the WP (i.e., 0.7 mm) is in the transition regime of emission, strong space-charge fields on the cathode surface play a major role leading to a prominent space-charge contribution to the emittance while the intrinsic contribution from the cathode is moderate. Decreasing the cathode laser spot size (toward 0.6 mm) causes further increase in the space-charge induced emittance and, therefore, blows up the overall emittance. On the contrary, increasing the spot size (toward 0.9 mm) relaxes the local space-charge density at the cathode and, thus, decreases the space-charge induced emittance. However, larger

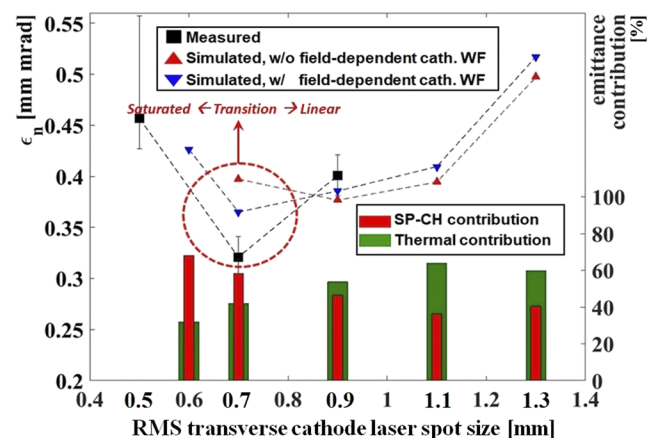


FIG. 7. Measurement and simulation of transverse beam emittance vs cathode laser spot size and analysis of the overall emittance budget in different emission regimes.

spot sizes on the cathode give larger intrinsic emittance. This leads to an increased overall emittance. It is, essentially, the interplay in the transition regime of emission, between the space-charge induced emittance and the intrinsic cathode emittance, which determines the optimized transverse emittance of the photoemitted electron beams. The strong space-charge fields play a key role at the cathode.

VI. CONCLUSION

In conclusion, the so-called transition regime of photoemission is identified and characterized in more detail. The presented experimental and numerical results suggest that operating the photoinjector in such a space-charge affected emission regime renders experimentally achievable best beam emittance for free-electron laser applications. An advanced beam dynamics modeling approach is proposed to consider the impacts of strong RF and beam self-fields in the cathode vicinity onto the beam dynamics. The overall emittance budget in the identified emission regime is analyzed in comparison with the space-charge induced emittance and the intrinsic cathode emittance. The simulation results are consistent with the measurement data. It can also be noted that resolving the complex beam dynamics due to strong space-charge forces in the cathode vicinity at the optimum working point of the accelerator requires detailed modeling of the photoemission process.

ACKNOWLEDGMENTS

The corresponding author would like to thank M. Dohlus and K. Floettmann from DESY and E. Gjonaj from TEMF, TU Darmstadt, for useful discussions. This work was supported by the European XFEL research and development program. The authors thank Dr. Hamed Shaker, Dr. Shankar Lal and David Melkumyan from DESY for helping with the PITZ facility operation.

REFERENCES

- W. Decking and H. Weise, "Commissioning of the European XFEL accelerator," in *Proceedings of the 8th International Particle Accelerator Conference, Copenhagen, May 2017* (JACoW, Geneva, Switzerland, 2017), pp. 1–6, paper No. MOXAA1.
- M. O. Wiedorn, D. Oberthür, R. Bean, R. Schubert, N. Werner *et al.*, *Nat. Commun.* **9**, 4025 (2018).
- B. Carlsten, "New photoelectric injector design for the Los Alamos National Laboratory XUV FEL accelerator," *Nucl. Instrum. Methods Phys. Res., Sect. A* **285**, 313–319 (1989).
- F. Stephan and M. Krasilnikov, "High brightness photo injectors for brilliant light sources," in *Synchrotron Light Sources and Free-Electron Lasers* (Springer International Publishing Switzerland, Switzerland, 2016).
- D. H. Dowell, I. Bazarov, B. Dunham, K. Harkay, C. Hernandez-Garcia, R. Legg, H. Padmore, T. Rao, J. Smedley, and W. Wan, "Cathode R&D for future light sources," *Nucl. Instrum. Methods Phys. Res., Sect. A* **622**, 685 (2010).
- N. A. Moody, K. L. Jensen, A. Shabaev, S. G. Lambrakos, J. Smedley, D. Finkenzadt, J. M. Pietryga, P. M. Anisimov, V. Pavlenko, E. R. Batista *et al.*, "Perspectives on designer photocathodes for x-ray free-electron lasers: Influencing emission properties with heterostructures and nanoengineered electronic states," *Phys. Rev. Appl.* **10**, 047002 (2018).
- M. Krasilnikov, F. Stephan, G. Asova, H.-J. Grabosch, M. Gross, L. Hakobyan, I. Isaev, Y. Ivanisenko, L. Jachmann, M. Khojayan *et al.*, "Experimentally minimized beam emittance from an L-band photoinjector," *Phys. Rev. Spec. Top.-Accel. Beams* **15**, 100701 (2012).
- F. Stephan, C. H. Boulware, M. Krasilnikov, J. Baehr, G. Asova, A. Donat, U. Gensch, H. J. Grabosch, M. Haenel, L. Hakobyan *et al.*, "Detailed characterization of electron sources yielding first demonstration of European x-ray free-electron laser beam quality," *Phys. Rev. Spec. Top.-Accel. Beams* **13**, 020704 (2010).
- Y. Chen, E. Gjonaj, H. D. Gersem, T. Weiland, M. Krasilnikov *et al.*, "Modeling and simulation of photoemission based electron sources," in *Proceedings of the International Computational Accelerator Physics Conference, Shanghai, October 2015* (JACoW, Geneva, Switzerland, 2015), pp. 157–159, paper No. THWC1.
- Y. Chen, paper presented at the 39th International Free-Electron Laser Conference, Hamburg, Germany, August 2019, paper No. WEA03.
- Y. Chen, M. Krasilnikov, F. Stephan, E. Gjonaj, T. Weiland, and M. Dohlus, "Modeling and simulation of RF photoinjectors for coherent light sources," *Nucl. Instrum. Methods Phys. Res., Sect. A* **889**, 129–137 (2018).
- Y. Chen, E. Gjonaj, W. Müller, and T. Weiland, "3D full electromagnetic beam dynamics simulations of the PITZ photoinjector," in *Proceedings of the 5th International Particle Accelerator Conference, Dresden, June 2014* (JACoW, Geneva, Switzerland, 2014), pp. 391–393, paper No. MOPME008.
- C. Hernandez-Garcia, M. Krasilnikov, G. Asova, M. Bakr, P. Boonpornprasert, J. Good, M. Gross, H. Huck, I. Isaev, D. Kalantaryan *et al.*, "Charge production studies from Cs₂Te photocathodes in a normal conducting RF gun," *Nucl. Instrum. Methods Phys. Res., Sect. A* **871**, 97–104 (2017).
- W. E. Spicer and A. Herrera-Gomez, "Modern theory and applications of photocathodes," SLAC-PUB-6306, 1993.
- K. L. Jensen, N. A. Moody, D. W. Feldman, E. J. Montgomery, and P. G. O'Shea, "Photoemission from metals and cesiated surfaces," *J. Appl. Phys.* **102**, 074902 (2007).
- K. L. Jensen, B. L. Jensen, E. J. Montgomery, D. W. Feldman, P. G. O'Shea, and N. Moody, "Theory of photoemission from cesium antimonide using an alpha-semiconductor model," *J. Appl. Phys.* **104**, 044907 (2008).
- J. Petillo, E. Nelson, J. DeFord, N. Dionne, and B. Levush, "Recent developments to the MICHELLE 2-D/3-D electron gun and collector modeling code," *IEEE Trans. Electron Devices* **52**, 742–748 (2005).
- Y. Chen, M. Krasilnikov, and F. Stephan, "The cooling effect of beam self-fields on the photocathode surface in high gradient RF injectors," in *Proceedings of the 10th International Particle Accelerator Conference, Melbourne, May 2019* (JACoW, Geneva, Switzerland, 2019), pp. 3112–3115, paper No. WEPTS013.
- E. Gjonaj, paper presented at the 11th International Computational Accelerator Physics Conference, Rostock-Warnemuende, Germany, August 2012.
- F. Ciocci, L. Giannessi, A. Marranca, L. Mezi, and M. Quattromini, "Self-consistent three-dimensional RF-gun dynamics integration based on the Lienard-Wiechert retarded potentials," *Nucl. Instrum. Methods Phys. Res., Sect. A* **393**, 434–438 (1997).
- R. Ryne, B. Carlsten, N. Yampolsky, C. Mitchell, and J. Qiang, "Using a Lienard-Wiechert solver to study coherent synchrotron radiation effects," in *Proceedings of the 35th International Free Electron Laser Conference, New York, August 2013* (JACoW, Geneva, Switzerland, 2013), pp. 17–19, paper No. MOOCN004.
- K. Floettmann, DESY-TESLA-FEL-97-06F, DESY, 1997.
- M. Krasilnikov, P. Boonpornprasert, Y. Chen, G. Georgiev, J. Good *et al.*, "PITZ experimental optimization for the aimed cathode gradient of a superconducting CW RF gun," in *Proceedings of the International Free Electron Laser Conference, Hamburg, August 2019* (JACoW, Geneva, Switzerland, 2019), p. WEP051.